# Dynamics of a one-dimensional Holstein polaron with Davydov Ansatze

Zhao, Yang; Sun, Jin; Luo, Bin

2010

Zhao, Y., Sun, J., & Luo, B. (2010). Dynamics of a one-dimensional Holstein polaron with Davydov Ansatze. Physical Review B: Condensed Matter and Materials Physics.

https://hdl.handle.net/10356/91744

# Dynamics of a one-dimensional Holstein polaron with Davydov Ansätze

Jin Sun, Bin Luo, and Yang Zhao*
*School of Materials Science and Engineering, Nanyang Technological University, Singapore 639798*
(Dated: February 22, 2010)

Following the Dirac-Frenkel time-dependent variational principle, dynamics of a one-dimensional Holstein polaron is probed by employing the Davydov $D_2$ Ansatz with two sets of variational parameters, one for each constituting particle in the exciton-phonon system, and a simplified variant of the Davydov $D_1$ Ansatz, also known as the $\tilde{D}$ Ansatz, with an additional set of phonon displacement parameters. A close examination of variational outputs from the two trial states reveals fine details of the polaron structure and intricacies of dynamic exciton-phonon interactions. Superradiance coherence sizes, speeds of exciton-induced phonon wave packets, linear optical absorption, and polaron energy compositions are also included in the study.

PACS numbers:

## I. INTRODUCTION

An electron in an insulating crystal induces a local lattice distortion around itself as it is excited by a photon. The electron together with the locally distorted lattice around it can be viewed as a quasiparticle which is also known as a polaron. Relaxation dynamics of photoexcited entities such as polarons in liquids and solids has recently received much interest thanks to the advent of the ultrafast laser spectroscopy[1–3]. It is now commonly accepted that dephasing and relaxation time scales in condensed matter are approximately picoseconds to tens of picoseconds. Emerging technological capabilities to control femtosecond pulse durations and down-to-one-hertz bandwidth resolutions provide novel probes on vibrational dynamics and excitation relaxation. For example, progress in femtosecond spectroscopic techniques has made it possible to observe a coherent phonon wave packet oscillating along an adiabatic potential surface associated with a self-trapped exciton in a crystal with strong exciton-phonon interactions[4].

Ultrafast events occur on femtosecond to picosecond timescales, and studies of ultrafast relaxation dynamics are a strategic research domain from both fundamental and technological points of view. It is the aim of an ultrafast optical experiment to provide information on the details of temporal evolution on a femtosecond scale, which, in turn, offers insights into fundamental processes governing the dynamics. Developments in ultrafast laser physics and technologies now allow studies of nonequilibrium carrier/exciton dynamics that is previously inaccessible to traditional linear optical spectroscopy. However, theoretical studies of polaron dynamics has not received much-deserved attention due to inherent difficulties in obtaining reliable solutions. Previously, a time-dependent form of the Merrifield-type polaron wave function with zero crystal momentum has been employed to yield an approximative solution to the Schrödinger equation that governs the ultrafast relaxation process of a one-dimensional molecular chain[5–8]. Results show that temporal changes of the exciton coherence size and related energy relaxation strongly depend on the exciton transfer integral, the exciton-phonon coupling strength, and the phonon bandwidth. The applicability of the Merrifield wave function, however, is restricted to the narrow-band regime where the electronic coupling between neighboring molecules is sufficiently weak leaving the electron-phonon coupling at a dominant role. In addition, in the presence of off-diagonal electron-phonon interactions, the Merrifield Ansatz is shown to fail[9].

Beyond the Merrifield Ansatz, there exist several trial wave functions of increasing sophistication to describe the polaron state in a translationally invariant manner such as the Toyozawa Ansatz[10], the Global-Local (GL) Ansatz formulated by Zhao and coworkers in the early 90s[11,12], and a delocalized form of the Davydov $D_1$ Ansatz that has been constructed very recently[13]. By using these Ansätze, we have previously investigated the ground state polaron energy band and the self-trapping phenomenon of a static Holstein polaron. Far superior results have been obtained compared with the Merrifield Ansatz[9,12,14]. Closely related to those polaron trial states are the Davydov Ansätze which originated from the theory of "Davydov soliton." Seeking to explain storage and transport of biological energy in protein structures, Davydov proposed in 1973 that quantum units of peptide vibrational energy might become "self-localized" through interactions with lattice phonons[15,16]. Following his suggestion, many related studies have been carried out on the "Davydov soliton," an essentially one-dimensional object that maintains dynamic integrity by balancing the effects of nonlinearity against those of dispersion. The original Davydov Ansätze include two forms of varying sophistication, namely, the $D_1$[17–23] and $D_2$ Ansätze, with the latter being a special case of the former.

In this work, we employ the Davydov $D_2$ Ansatz and a localized form factor of the GL Ansatz, previously known as the $\tilde{D}$ Ansatz, to study time evolution of the Holstein polaron following the Dirac-Frenkel time-dependent vari-

*Electronic address: YZhao@ntu.edu.sg

ational approach[24]. Time-dependent variational parameters which specify the two Ansätze are obtained from solving a set of coupled differential equations generated by the Lagrangian formalism of the Dirac-Frenkel variation. Special attention is paid to the evolution of the reduced single-exciton density matrix and the propagation of exciton and phonon amplitudes from an initial location, where the exciton resides at $t = 0$, to the entire aggregate.

The paper is organized as follows. In Sec. II we introduce the model Hamiltonian and discuss the nature of the trial states we use for dynamics studies, which is followed by the procedure of the time-dependent variation. In Sec. III results from our dynamics calculation using the two trial states are displayed and discussed. Conclusions are drawn in Sec. IV.

## II. METHODOLOGY

We consider a one-dimensional aggregate of N molecules with a periodic boundary condition. There is only one two-level electronic system for each molecule coupled linearly with the phonon field. The Holstein Hamiltonian for the exciton-phonon system can be written as[25–27]

$$\hat{H} = \hat{H}_{\rm ex} + \hat{H}_{\rm ex-ph} + \hat{H}_{\rm ph} \tag{1}$$

with

$$\hat{H}_{\rm ex} = -J\sum_n \hat{B}_n^\dagger(\hat{B}_{n+1} + \hat{B}_{n-1}) \tag{2}$$

$$\hat{H}_{\rm ph} = \sum_q \omega_q \hat{b}_q^\dagger \hat{b}_q \tag{3}$$

$$\hat{H}_{\rm ex-ph} = \sum_{q,n=1}^{N} g_q\omega_q \hat{B}_n^\dagger \hat{B}_n(\hat{b}_q e^{iqn} + \hat{b}_q^\dagger e^{-iqn}) \tag{4}$$

Here $\hat{H}_{\rm ex}$ is the Hamiltonian for a single Frenkel exciton band in a rigid chain, and $\hat{B}_n(\hat{B}_n^\dagger)$ is the Pauli annihilation (creation) operator of an exciton at the $n$th site. We set $\hbar = 1$ and assume the nearest-neighbor exciton transfer integral $J_{mn} = J\delta_{m,n\pm1}$. $\hat{H}_{\rm ph}$ is the phonon Hamiltonian where $\hat{b}_q(\hat{b}_q^\dagger)$ is the boson annihilation (creation) operator of a phonon with monentum $q$ and frequency $\omega_q$. For simplicity, the zero-point energy is neglected. $\hat{H}_{\rm ex-ph}$ assumes the exciton is coupled linearly with the phonon field in a site diagonal form.

Because there is no exciton in the ground state, the Hamiltonian for the ground state is represented by

$$\hat{H}_{\rm g} = |0\rangle_{\rm ex}\ \hat{H}_{\rm ph}\ {}_{\rm ex}\langle 0| \tag{5}$$

where $|0\rangle_{\rm ex}$ stands for the exciton vacuum. The global ground state is then described as a direct product of both vacuum states of the exciton and the phonon field: $|G\rangle = |0\rangle_{\rm ex}|0\rangle_{\rm ph}$. We confine ourselves to one-exciton subspace for the optically excited state[28] since the exciton number is conserved in the total Hamiltonian in Eq. (1).

The spectral density[29] embodying all relevant information of the coupled exciton-phonon system in Eq. (4) can be written as

$$C_{mn}(\omega) \equiv \frac{1}{2\pi}\int_{-\infty}^{\infty}\langle \hat{V}_m(t)\hat{V}_n(0)\rangle_{\rm ph} e^{i\omega t}dt \tag{6}$$

where $\hat{V}_n(t)$ is a Heisenberg representation of the exciton-phonon interaction at the $n$th site

$$\hat{V}_n = \sum_q g_q\omega_q e^{iqn}(\hat{b}_q + \hat{b}_{-q}^\dagger) \tag{7}$$

and the $\langle\cdots\rangle_{\rm ph}$ denotes the thermal average in the free-phonon basis. Note that $C_{mn}(\omega)$ represents not only the time correlation but also the spatial correlation for the exction-phonon interactions[29]. Here only the case of zero temperature is considered. Substituting Eq. (7) into Eq. (6), one has

$$C_{mn}(\omega) = \sum_q g_q^2\omega_q^2 e^{iq(m-n)}\delta(\omega - \omega_q) \tag{8}$$

Following Tanaka[8], the spectral density is assumed to have the form

$$\begin{aligned} C_{00}(\omega) &= \sum_q g_q^2\omega_q^2\delta(\omega-\omega_q) \\ &= \frac{2S\omega^2}{\pi W^2}\sqrt{W^2-(\omega-\omega_0)^2} \end{aligned} \tag{9}$$

The relaxation energy is defined by

$$E_r \equiv \int_{-\infty}^{\infty}\frac{C_{00}(\omega)}{\omega}d\omega = \sum_q g_q^2\omega_q \equiv S\omega_0 \tag{10}$$

where $S$ is the Huang-Rhys factor[30], $\omega_0$ is the central energy of the phonon band, and $W$ is the phonon energy band width . Here we assume a linear dispersion phonon band with a linear dispersion

$$\omega_q = \omega_0 + 2W(\frac{|q|}{\pi} - \frac{1}{2}) \tag{11}$$

The central frequency of the phonon band $\omega_0$ is taken as the energy unit, i.e., $\omega_0 = 1$. From Eqs. (9)-(11), we can obtain $g_q$ for a given $S$ and $W$.

The Merrifield Ansatz, also known as the small-polaron Ansatz[5,6], is a simple, effective trial state to describe a coupled exciton-phonon system in which the exciton transfer integral is small compared with other system energy scales. There is only one set of variational parameters, the phonon displacements $\beta_n^K(t)$, or alternatively,

its Fourier transform $\beta_q^K(t)$, that characterizes the Merrifield trial state $|\Psi_{\rm M};K\rangle$ of crystal momentum $K$:

$$\begin{aligned}|\Psi_{\rm M};K\rangle &= N^{-1/2}\sum_n e^{iKn}|n\rangle_{\rm ex}\\ &\quad\times\exp[-\sum_{n_b}(\beta^K_{n_b-n}\hat{b}^\dagger_{n_b}-\beta^{K*}_{n_b-n}\hat{b}_{n_b})]|0\rangle_{\rm ph}\\ &= N^{-1/2}\sum_n e^{iKn}|n\rangle_{\rm ex}\\ &\quad\times\exp[-\sum_q(\beta^K_q e^{-iqn}\hat{b}^\dagger_q-\beta^{K*}_q e^{iqn}\hat{b}_q)]|0\rangle_{\rm ph}\end{aligned} \tag{12}$$

In contrast, Davydov built a theory of enveloped solitons based on the two trial states of localized nature

$$|D_1(t)\rangle\equiv\sum_n\psi_n(t)\hat{B}^\dagger_n|0\rangle_{\rm ex}\otimes|\lambda_n(t)\rangle \tag{13}$$

with

$$|\lambda_n(t)\rangle\equiv\exp\{\sum_q[\lambda_{qn}(t)\hat{b}^\dagger_q-\lambda^*_{qn}(t)\hat{b}_q]\}|0\rangle_{\rm ph} \tag{14}$$

and

$$|D_2(t)\rangle\equiv\sum_n\psi_n(t)\hat{B}^\dagger_n|0\rangle_{\rm ex}\otimes|\lambda(t)\rangle \tag{15}$$

with

$$|\lambda(t)\rangle\equiv\exp\{\sum_q[\lambda_q(t)\hat{b}^\dagger_q-\lambda^*_q(t)\hat{b}_q]\}|0\rangle_{\rm ph} \tag{16}$$

The $D_1$ Ansatz differs from the more widely used $D_2$ Ansatz. In the $D_2$ Ansatz the phonon amplitudes are exciton-site independent, i.e., $\lambda_{qn}(t)=\lambda_q(t)$ for all n. The $D_2$ Ansatz reprsents the quantum state of each phonon mode by a single coherent state, and hence has at all times a strongly classical character. In such solutions, the typically pulse-shaped distribution of the amplitudes $\lambda_q$ describes a lattice deformation fixed in the frame of the lattice, to which conforms a correspondingly pulse-shaped distribution of exciton amplitudes $\psi_n$.

Since the description of phonons in the $D_2$ Ansatz is unsophisticated, direct correlations between the amplitudes of phonons and exciton are neglected. In many cases, the $D_2$ Ansatz is inadequate to capture the complexities of the exciton-phonon system. Therefore, we introduce the $\tilde{\rm D}$ Ansatz, i.e., the localized form factor of the GL Ansatz:

$$\begin{aligned}|\tilde{D}(t)\rangle &= \sum_{n_1}\psi_{n_1}(t)\hat{B}^\dagger_n\exp[\sum_{n_2}(\lambda_{n_2}-\beta_{n_2-n_1})\hat{b}^\dagger_{n_2}\\ &\quad-(\lambda^*_{n_2}-\beta^*_{n_2-n_1})\hat{b}_{n_2}]|0\rangle\\ &= \sum_n\psi_n(t)\hat{B}^\dagger_n\exp[N^{-1/2}\sum_q(\beta_q e^{-iqn}-\lambda_q)\hat{b}^\dagger_q\\ &\quad-(\beta^*_q e^{iqn}-\lambda^*_q)\hat{b}_q]|0\rangle\end{aligned} \tag{17}$$

The global amplitude $\lambda_q$ can be related to the spatial average of $\lambda_{qn}$ , and the local amplitude $\beta_q e^{-iqn}$ can be viewed as an Ansatz for the spatial variation of $\lambda_{qn}$ around this mean value.

The time evolution of the photoexcited state in a one-dimensional molecular aggregate follows the time-dependent Schrödinger equation. As far as the exciton-phonon coupling is weak, it can be treated perturbatively leading to a nonlinear exciton equation with the use of the relaxation superoperator. In the strong coupling case, however, the perturbative method is no longer valid. There are several approaches to solve the time-dependent Schrödinger equation. In the Hilbert space, the time-dependent wave function $|\Phi(t)\rangle$ for the Hamiltonian $\hat{H}$ is parameterized by $\alpha_m(t)$ $(m=1,...,M)$:

$$|\Phi(t)\rangle\equiv|\{\alpha_m(t)\}\rangle. \tag{18}$$

Assume that $|\Phi(t)\rangle$ satisfies the time-dependent Schrödinger equation

$$i\frac{\partial}{\partial t}|\Phi(t)\rangle=\hat{H}|\Phi(t)\rangle. \tag{19}$$

Explicitly putting in the Hamiltonian $\hat{H}$ of Eq. (1) and writing $\partial|\Phi(t)\rangle/\partial t$ in terms of $\alpha_m(t)$ and their time-derivatives $\dot{\alpha}_m(t)$ $(m=1,...,M)$, one has

$$i\frac{\partial}{\partial t}|\{\alpha_m(t)\}\rangle=\hat{H}|\{\alpha_m(t)\}\rangle \tag{20}$$

Projecting Eq. (20) onto $M$ different states $|\Psi_m\rangle$ $(m=1,...,M)$, one obtains $M$ equations of motion for the parameters $\alpha_m(t)$:

$$\langle\Psi_m|\{\alpha_m(t)\},\{\dot{\alpha}_m(t)\}\rangle=0 \tag{21}$$

The approach we adopt in this work is the Lagrangian formalism of the Dirac-Frenkel time-dependent variational method[31], a powerful technique to obtain approximate dynamics of many-body quantum systems for which exact solutions often elude researchers. We formulate the Lagrangian $L$ as follows

$$L=\langle\Phi(t)|\frac{i\hbar}{2}\frac{\overleftrightarrow{\partial}}{\partial t}-\hat{H}|\Phi(t)\rangle \tag{22}$$

From this Lagrangian, equations of motion for $\alpha_m(t)$ and their time-derivatives $\dot{\alpha}_m(t)$ $(m=1,...,M)$ can then be obtained

$$\frac{d}{dt}(\frac{\partial L}{\partial\dot{\alpha}^*_m})-\frac{\partial L}{\partial\alpha^*_m}=0 \tag{23}$$

It can be shown that with a properly chosen set of $|\Psi_m\rangle$, Eqs. (21) and (23) can coincide. The reader is referred to Appendices A, B and C where details of derivation together with these $M$ equations for $D_2$, $\tilde{\rm D}$ and $D_1$ Ansätze are given, respectively. Descriptions of the numerical procedure can be found in Appendix D.

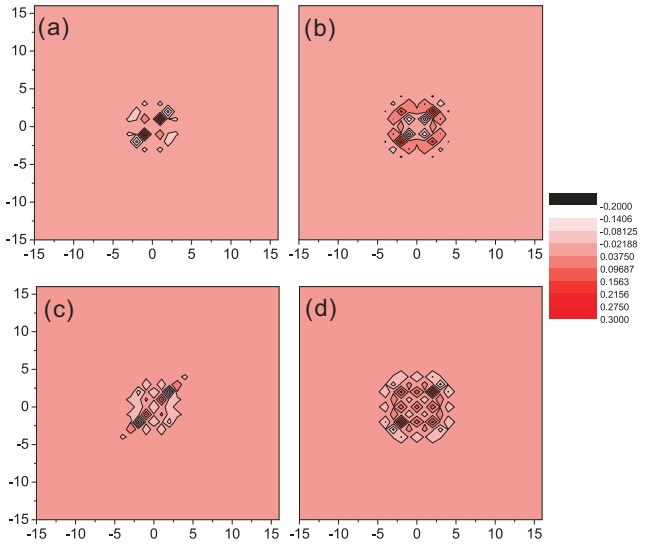


FIG. 1: The reduced exciton density matrix $\rho_{mn}$ calculated from the $\tilde{\mathrm{D}}$ Ansatz for (a) $t = 7\pi/\omega_0$; (b) $t = 8\pi/\omega_0$; (c) $t = 9\pi/\omega_0$; (d) $t = 10\pi/\omega_0$. The control parameters are $J = 0.1, W = 0.1$ and $S = 0.5$.

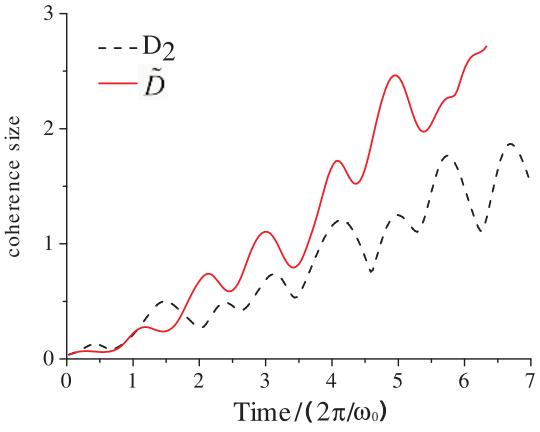


FIG. 2: The superradiance coherence size of the polaron $L_\rho$ for $J = 0.1$, $W = 0.1$ and $S = 0.5$ calculated from the $\tilde{\mathrm{D}}$ (solid) and $\mathrm{D}_2$ (dashed) Ansätze.

## III. RESULTS AND DISCUSSIONS

### A. Reduced Exciton Density Matrix and Coherence Size

The reduced single-exciton density matrix $\rho_{mn}(t)$ can be obtained after solving the coupled equations of variational parameters

$$\rho_{mn}(t) = \mathrm{Tr}[\rho(t)\hat{B}_m^\dagger \hat{B}_n] \tag{24}$$

where $\rho(t) = |\Phi(t)\rangle\langle\Phi(t)|$ is the full density matrix at zero temperature, and $|\Phi(t)\rangle$ is the total polaron wave function at time $t$ after the photo excitation takes place. Substituting the detailed form of the $\mathrm{D}_2$ Ansatz into the polaron wave function, one obtains

$$\rho_{mn} = \langle D_2|\hat{B}_m^\dagger \hat{B}_n|D_2\rangle = \psi_m^*(t)\psi_n(t) \tag{25}$$

For the $\mathrm{D}_2$ Ansatz, the reduced exciton density matrix involves only the exciton amplitude, and does not contain information of the phonon manifold. In contrast, the more sophisticated trial state, the $\tilde{\mathrm{D}}$ Ansatz, includes the Debye-Waller factor $S_{n,m}$ in the expression of the reduced exciton density matrix:

$$\rho_{mn} = \langle \tilde{D}|\hat{B}_m^\dagger \hat{B}_n|\tilde{D}\rangle = \lambda_m^*(t)\lambda_n(t)S_{m,n} \tag{26}$$

where $S_{n,m}$ can be written as

$$\begin{aligned} S_{n,m} \;=\; & \exp[-\frac{1}{2}N^{-1}\sum_q |\beta_q e^{-iqn} - \lambda_q|^2] \\ & \exp[N^{-1}\sum_q (\beta_q^* e^{iqn} - \lambda_q^*)(\beta_q e^{-iqm} - \lambda_q)] \\ & \exp[-1/2N^{-1}\sum_q |\beta_q e^{-iqm} - \lambda_q|^2] \end{aligned} \tag{27}$$

Using the Merrifield Ansatz[8], when $J = 0$, solutions to coupled equations of variational parameters can be obtained analytically for zero phonon bandwidth ($W = 0$). It is found that $L_\rho = 1/N$ for all $t = 2\pi n/\omega_0$ ($n = 1, 2, 3, ...$). Periodic changes of the polaron structure as a function of time have also been revealed when $J$ and $W$ are both small. At $\omega_0 t = 7\pi, 8\pi, 9\pi$ and $10\pi$, the reduced exciton density matrix $\rho_{mn}$ calculated from the $\tilde{\mathrm{D}}$ Ansatz for the case of $J = 0.1, W = 0.1$ and $S = 0.5$ is displayed in Fig. 1. At $t = 0$, $\rho_{mn}$ is confined to the $(0, 0)$ point, i.e., the exciton is localized at one site of the one-dimensional system. Then, as the excited state relaxes, the non-zero elements of $\rho_{mn}$ spread out gradually. Oscillatory behavior is visible during the evolution of the density matrix as both the $J$ and $W$ are small, and as a result, dephasing due to phonon dispersion and exciton transfer is at a minimal level. When $t$ equals to $2n\pi/\omega_0$, the matrix is rather delocalized and have a symmetric distribution, and at $t = (2n + 1)\pi/\omega_0$, matrix elements aggregate along the diagonal line.

When $J$ is increased, the oscillatory behavior of the density matrix gradually fades as the exciton density delocalization happens more swiftly. From the reduced exciton density matrix, one can obtain an exciton coherence size $L_\rho$[32–34] characterizing the size of a domain within which the chromophores emit coherently. All information relevant to the excitonic superradiance is contained within the reduced exciton density matrix $\rho_{mn}(t)$, the time dependence of which provides a clear view of the relaxation process. Previously, for translationally invariant states, a definition of the characteristic coherence size $L_\rho$ in terms of the density matrix was introduced by applying the inverse participation ratio concept commonly used in the theory of quantum localization:

$$L_\rho \equiv [L_0 \sum_{mn} |\rho_{mn}|^2]^{-1}[(\sum_{mn} |\rho_{mn}|)^2] \tag{28}$$

This definition of the coherence size is borrowed to quan-

tify the excitonic delocalization despite that our trial states are both of the localized form. Values of $L_\rho$ calculated from the $D_2$ and $\tilde{D}$ trial states for the case of $J = 0.1, W = 0.1$ and $S = 0.5$ are shown in Fig. 2 as a function of time. At $t = 0$, the coherence size is $1/32$ because the exciton is localized to one site completely. Then coherence size will increase in an oscillatory fashion. When $t$ equals $2n\pi/\omega_0$, the coherence size will reach a local maximum and then decrease until $t$ equals $(2n+1)\pi/\omega_0$. This is consistent with the time evolution of the reduced exciton density matrix.

### B. Exciton Amplitudes and Phonon Displacements of the $D_2$ Ansatz

At variance with the single-parameter Merrifield Ansatz, the localized $D_2$ trial state employs two sets of variational parameters for independent descriptions of the two types of constituting particles in the coupled exciton-phonon system. By studying the outputs of time-dependent variational parameters, namely, the exciton amplitude $\psi_n(t)$ and phonon displacement $\lambda_n(t)$, one is able to probe the polaron dynamics which follows photo-excitation at a single site of a one-dimensional molecular chain. At $t = 0$, it is assumed that the exciton is generated on one site and there are no initial phonon displacements on the chain. Thanks to the exciton transfer integral and the exciton-phonon coupling in the Holstein Hamiltonian, one witnesses the spreading of the exciton amplitude and the growth of phonon deformations around the initial exciton site. Here we use three examples to illustrate the time evolution of the exciton amplitude and the phonon displacement of the $D_2$ Ansatz in the site space. As shown in Figs. 3, 4 and 5 for three sets of $(J, W)$, $(0.5, 0.8), (0.5, 0.1)$ and $(1.0, 0.8)$ respectively, the exciton amplitude propagates from the initial site $n = 0$ to the entire chain with a speed that is propor-

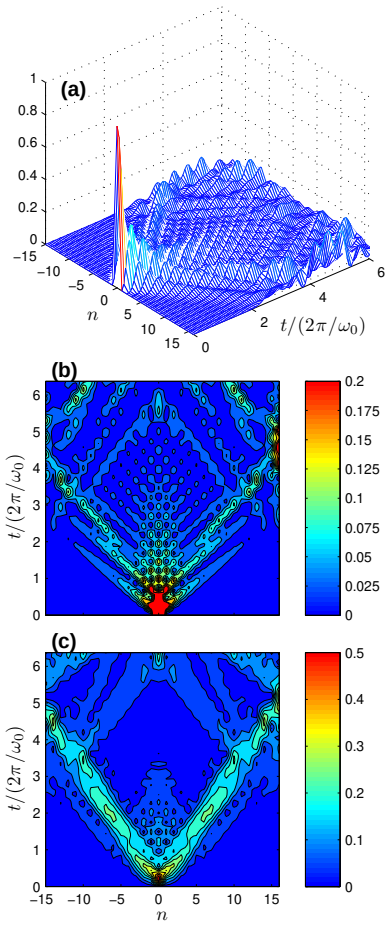


FIG. 3: Time evolution of variation parameters of the $D_2$ Ansatz for $J = 0.5$, $W = 0.8$ and $S = 0.5$. (a) A bird's-eye view of the exciton probability $|\psi_n(t)|^2$ in real space; (b) a contour plot of $|\psi_n(t)|^2$; (c) a contour plot of the phonon displacement $|\lambda_n(t)|$ in real space.

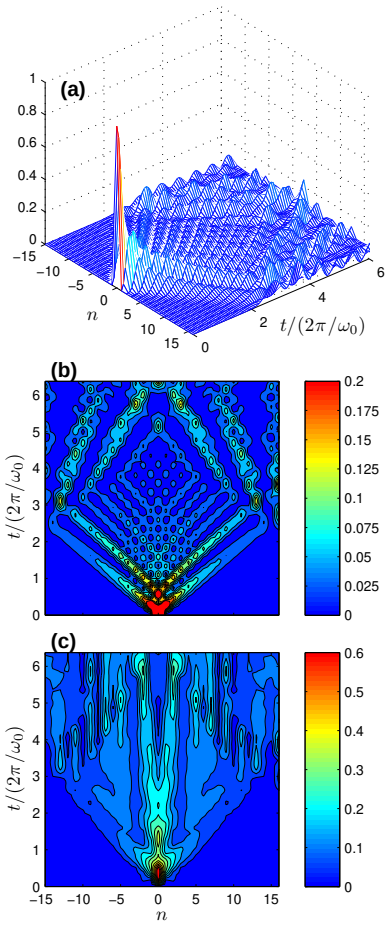


FIG. 4: Time evolution of variation parameters of the $D_2$ Ansatz for $J = 0.5$, $W = 0.1$ and $S = 0.5$. (a) A bird's-eye view of the exciton probability $|\psi_n(t)|^2$ in real space; (b) a contour plot of $|\psi_n(t)|^2$; (c) a contour plot of the phonon displacement $|\lambda_n(t)|$ in real space.

tional to the transfer integral $J$. The Huang-Rhys factor $S$ is set at 0.5. In Figs. 3 and 4 ($J = 0.5$), the first traveling wave of the exciton amplitude reaches the the opposite end of the ring ($n = 16$) at $t \approx 2.6(2\pi/\omega_0)$, while in Fig. 5 ($J = 1.0$), the exciton amplitude reaches the $n = 16$ site at $t \approx 1.3(2\pi/\omega_0)$. This is because the propagation speed of the exciton, or equivalently, $\partial E_{\rm ex}(k)/\partial k$ with $E_{\rm ex}(k)$ the bare exciton band, is proportional to the exciton transfer integral $J$ according to Eq. (2). The effect of phonon dispersion on the exciton is reflected in the differing degree of phonon-induced dissipation in Figs. 3b and 4b. Exciton wave packets in Fig. 4b survive much longer than those in Fig. 3b thanks to a much smaller phonon band width.

At $t = 0$ there are no phonon deformations anywhere on the one-dimensional ring. Due to photo-excitation at $t = 0$, a high concentration of the exciton density at a single location, appears in the vicinity of $n = 0$ for a short time duration near $t = 0$ [the red-colored spot near the point $(0, 0)$ in Figs. 3b, 4b and 5b], triggering a pair of localized phonon wave packets which travel at group velocities $\pm v_q$ with

$$v_q = \nabla_q \omega_q = \frac{2W}{\pi}. \tag{29}$$

As shown in Figs. 3c, 4c and 5c, the angle between the two trajectories of phonon wave packets departing from point $(0, 0)$ but with opposite velocities in Figs. 3c and 5c ($W = 0.8$) is about 8 times of that in Fig. 4c ($W = 0.1$).

For a larger value of transfer integral, e.g., $J = 1.0$ in Fig. 5, the left-moving and right-moving wave packets of the exciton depart the site of creation and makes a quick rendezvous at the opposite site of the ring ($n = 16$), where the recombined exciton density remains sufficiently high to trigger another pair of localized phonon wave packets as is clearly demonstrated in Figs. 5b and 5c. The exciton will travel at a much reduced speed after the rendezvous at $n = 16$, and further stimulations of phonon wave packets are all but impossible for $J = 1.0$.

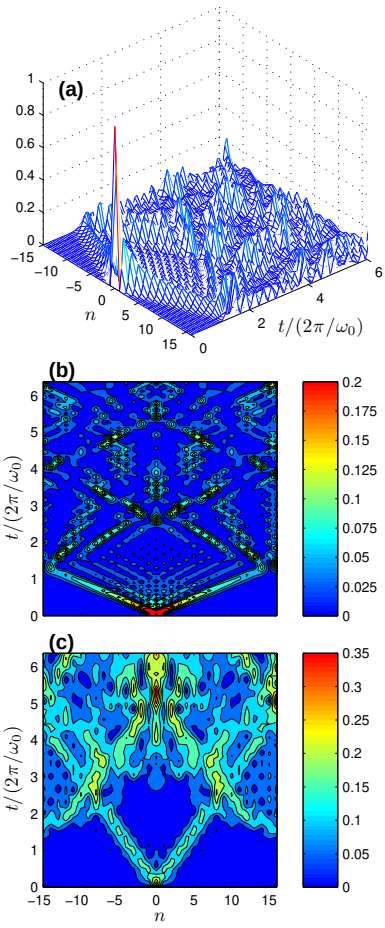


FIG. 5: Time evolution of variation parameters of the $D_2$ Ansatz for $J = 1.0$, $W = 0.8$ and $S = 0.5$. (a) A bird's-eye view of the exciton probability $|\psi_n(t)|^2$ in real space; (b) a contour plot of $|\psi_n(t)|^2$; (c) a contour plot of the phonon displacement $|\lambda_n(t)|$ in real space.

### C. Vibrational Amplitude of Exciton and Phonon using $\tilde{\rm D}$ Ansatz

In Figs. 6, 7 and 8, time evolution of the variational parameters $|\psi_n(t)|^2$, $|\lambda_n(t)|$ and $|\lambda_n(t)|$ is displayed for the $\tilde{\rm D}$ Ansatz. When $J$ and $W$ are both small, the phonons are mostly localized in the vicinity of the site where the exciton is initially created. The first set of phonon displacements, $|\lambda_n(t)|$, will extend slightly to the neighboring sites as the time increases because of a nonzero $J$ and a finite phonon dispersion (Fig. 7a). But as shown in Fig. 8a, there is almost no spreading of $\beta_n(t)$, suggesting that this portion of phonon displacements closely follows the exciton and appears almost entirely on the site of exciton creation. Fig. 8a also reveals oscillatory behavior of $|\beta_n(t)|$: when $t$ equals $(2n + 1)\pi/\omega_0$, $|\beta_n(t)|$ reaches its maximum value; and when $t$ equals $2n\pi/\omega_0$, the amplitude is at its minimum. Because the transfer integral $J$ is nearly zero, the exciton stays very close to the site of creation. From Fig. 6a, it is obvious that the exciton stays localized on one site with hardly any propagation for a small value of transfer integral $J = 0.1$. In this case, it seems that oscillations of phonon amplitudes also influence the movement of the exciton. The propagation of the exciton from the $n = 0$ site to its nearest neighbors occurs only at $t = 2n\pi/\omega_0$ when the phonon amplitude reaches a minimum value. Otherwise, because of the coupling with the phonons, the exciton will be trapped and unable to transfer to other sites.

As $J$ is increased, the exciton will have the ability to move away from the site of creation. As shown in Figs. 6b and 6d, the larger $J$ is, the faster the exciton transfers. Although $J$ has no direct influence over the phonon displacements, a large $J$ induces more excitonic coherence between adjacent sites, and in turn, causes more phonon deformations on those sites (cf. Fig. 7). The propagation

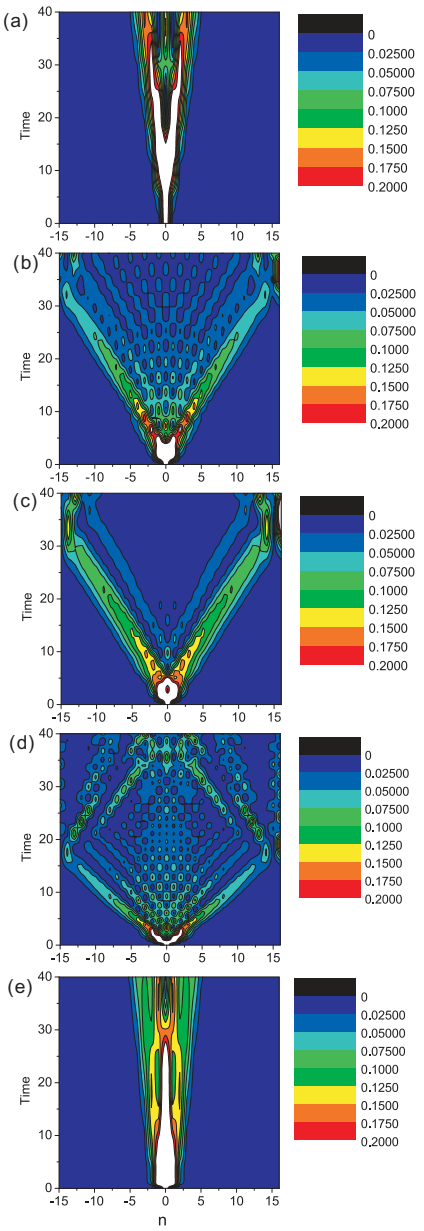


FIG. 6: Time evolution of the exciton probability $|\psi_n(t)|^2$ in real space using $\tilde{\mathrm{D}}$ Ansatz. The unit of time is $1/\omega_0$. (a) $J = 0.1,\ W = 0.1,\ S = 0.5$; (b) $J = 0.5,\ W = 0.8,\ S = 0.5$; (c) $J = 0.5,\ W = 0.1,\ S = 0.5$; (d) $J = 1.0,\ W = 0.8,\ S = 0.5$; (e) $J = 1.0,\ W = 0.8,\ S = 2.0$.

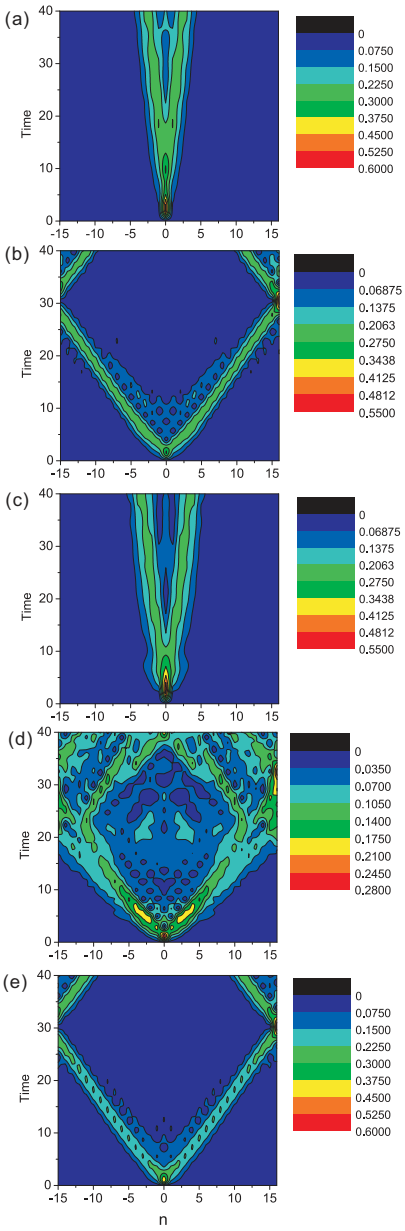


FIG. 7: Time evolution of the phonon displacements $|\lambda_n(t)|$ of the $\tilde{\mathrm{D}}$ Ansatz in real space. The unit of time is $1/\omega_0$. (a) $J = 0.1,\ W = 0.1,\ S = 0.5$; (b) $J = 0.5,\ W = 0.8,\ S = 0.5$; (c) $J = 0.5,\ W = 0.1,\ S = 0.5$; (d) $J = 1.0,\ W = 0.8,\ S = 0.5$; (e) $J = 1.0,\ W = 0.8,\ S = 2.0$.

of the localized phonon wave packets related to $\beta_n(t)$ becomes faster $J$ is increased from 0.5 to 1.0 as shown in Fig. 8.

As for the $\tilde{\mathrm{D}}$ Ansatz, an increase in the width of the phonon dispersion $W$ will substantially deepen the phonon dissipative effect on the exciton amplitude $\psi_n(t)$, and as a result the exciton coherence quickly vanishes from the case of $W = 0.8$. (cf. Fig. 6b and 6c). $W$ is also one main factor which determines the velocity of the phonon wave packets for both types of phonon displacements $\lambda_n(t)$ and $\beta_n(t)$. Fig. 7c shows that when $W$ is small, most of $\lambda_n(t)$ will be localized on the $n = 0$ site. As the phonon band width increases, $\lambda_n(t)$ will form two traveling wave packets with opposite directions and propagate to the entire chain as shown in Fig. 7b.

The dynamics of $\beta_n(t)$ is more complex. As shown in Figs. 7b and 7c, the phonon displacements described by parameter $\lambda_n(t)$ propagate from the $n = 0$ site to the rest of the aggregate. But the same is not true for $\beta_n(t)$. Most of $\beta_n(t)$ will stay localized on the site of exciton

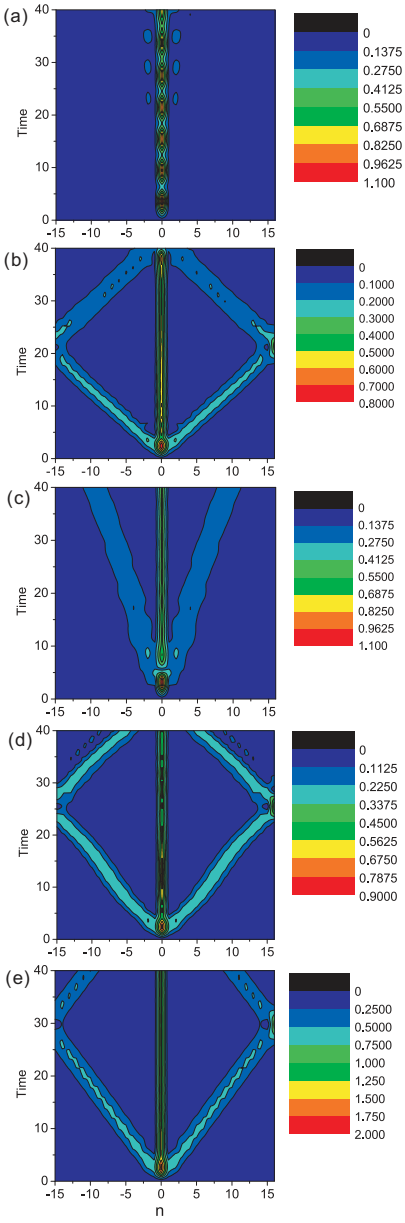


FIG. 8: Time evolution of the phonon vibrational amplitude $|\beta_n(t)|$ in real space using $\tilde{\mathrm{D}}$ Ansatz. The unit of time is $1/\omega_0$. (a) $J = 0.1,\ W = 0.1,\ S = 0.5$; (b) $J = 0.5,\ W = 0.8,\ S = 0.5$; (c) $J = 0.5,\ W = 0.1,\ S = 0.5$; (d) $J = 1.0,\ W = 0.8,\ S = 0.5$; (e) $J = 1.0,\ W = 0.8,\ S = 2.0$.

creation, but we can also find a small portion of $\beta_n(t)$ propagating to the entire molecular chain as we increase $W$ (cf. Fig. 8b and 8c). From the definition of the $\tilde{\mathrm{D}}$ Ansatz, Eq. (17), $\beta_n(t)$ represents the portion of phonon displacements that ride along the exciton, while $\lambda_n(t)$ labels the phonon displacements that are not explicitly linked to the exciton. We therefore expect that the propagation speeds of the localized phonon wave packets from the two types of phonon displacements $\lambda_n(t)$ and $\beta_n(t)$ are different. But both of them depend on the $W$ linearly, and the slopes are found to be the same, as shown in Fig. 9.

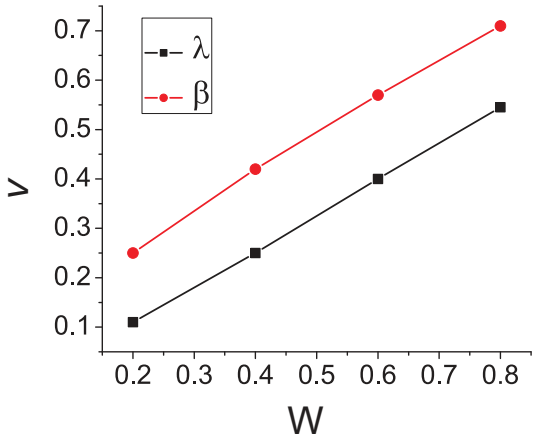


FIG. 9: Speeds of localized phonon wave packets as a function of the half width of the phonon dispersion $W$ for the two sets of phonon displacements $\lambda_n(t)$ (in black) and $\beta_n(t)$ (in red). $J = 0.5,\ S = 0.5$.

Lastly, we examine the effect of the Huang-Rhys factor $S$ which is a dimensionless parameter representing the exciton-phonon coupling strength. $S$ can be obtained directly from absorption and fluorescence spectra, as it controls the vibrational progression that accompanies an exciton transition. Comparing Fig. 6d with Fig. 6e, the exciton is found to be much less mobile as $S$ is increased from 0.5 to 2.0, undergoing the so-called self-trapping transition. The fact that Fig. 6d displays a much faster-moving polaron than Fig. 6e is also reflected in Fig. 8d, in which the localized phonon wave packet in $\beta_n(t)$ is found to be much longer-lasting than that in Fig. 8e, and its speed greater. In addition, Fig. 7d shows a few scattered localized phonon wave packets of $\lambda_n(t)$, while Fig. 7e contains only a single localized phonon wave packet of $\lambda_n(t)$.

### D. Absorption Spectra and System Energies

Details on how to calculate linear absorption spectra of a one-dimensional exciton-phonon system from the $\mathrm{D}_2$ and $\tilde{\mathrm{D}}$ Ansätze can be found in Appendix E. Fig. 10a and 10b show two examples of the spectra get by $\mathrm{D}_2$ Ansatz and $\tilde{\mathrm{D}}$ Ansatz, respectively, and the results are compared with those from the Merrifield Ansatz. As shown in Fig. 10a, when $J$ is small (e.g., $J = 0.1$) and $S$ is large (e.g., $S = 6.0$), the spectra obtained by the $\mathrm{D}_2$ and Merrifield Ansätze are almost the same. The phonon sidebands in Fig. 10a is labeled by $n = 0, 1, 2, ...$ from left to right. The left most sideband, $n = 0$, corresponding to the zero-phonon line, is located at $\omega = -S\omega_0$ [Eq. (10)]. For $S = 6.0$, the zero-phonon line is located at $\omega = -6\omega_0$ as shown in Fig. 10a. According to the Huang-

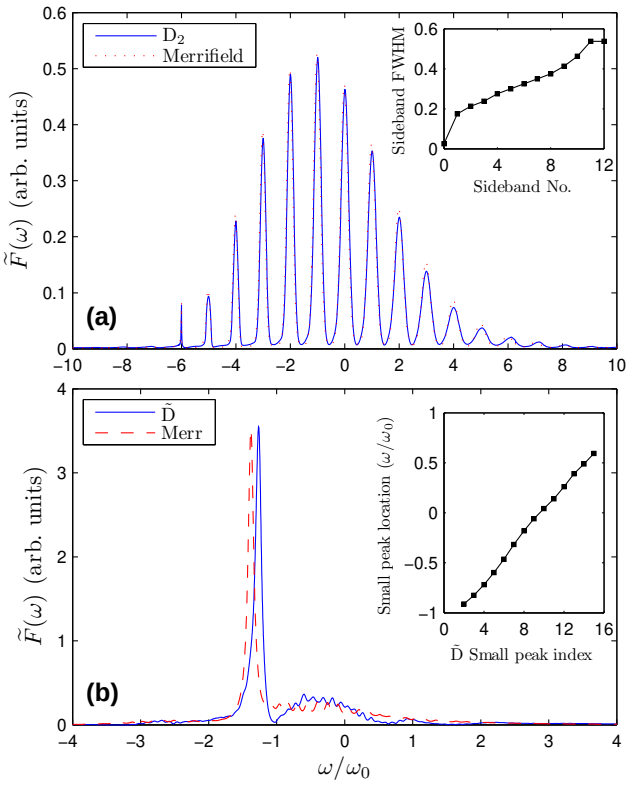


FIG. 10: Linear absorption spectra of a 32-site one-dimensional ring of a coupled exciton-phonon system. (a) Using the $D_2$ and Merrifield Ansätze for $J = 0.1$, $W = 0.1$ and $S = 6.0$. The decay factor used in the Fourier transformation is 0.01. (b) Using the $\tilde{D}$ and Merrifield Ansätze for $J = 0.4$, $W = 0.8$ and $S = 1.0$. The decay factor used in the Fourier transformation is 0.05.

Rhys theory[30], the phonon sidebands at zero temperature follow a Poisson distribution:

$$\widetilde{F}_{\rm abs}(\omega) = \exp(-S)\sum_{n=0}^{\infty}\frac{S^n}{n!}\delta(\omega + E_r - n\omega_0) \qquad (30)$$

From Eq. (30), the tallest of phonon sidebands should be the $n = S - 1$ peak when $S \gg 1$ and the overall distribution approaches a Gaussian. Thus, for $S = 6.0$, the tallest peak is at $n = 5$ as shown in Fig. 10a.

Fig. 10b displays the absorption spectrum calculated from the $\tilde{D}$ and Merrifield Ansätze for $J = 0.4$, $W = 0.8$ and $S = 1.0$. There are fine features with tiny peaks on the one-phonon manifold on the right side of the zero-phonon line. These small peaks are attributed to the 32 phonon modes with momenta $q = 2\pi n_q/N$ ($N = 32$; $n_q = -15, -14, ..., 14, 15, 16$). As in this paper we assume a linear phonon dispersion as defined in Eq. (11), there are altogether 17 values of $\omega_q$ for $N = 32$. Each value of $\omega_q$ should correspond to a small peak on the spectrum if the coupling $g_q$ [Eq. (7)] is not too small, and from Eq. (11), one can obtain the locations of the

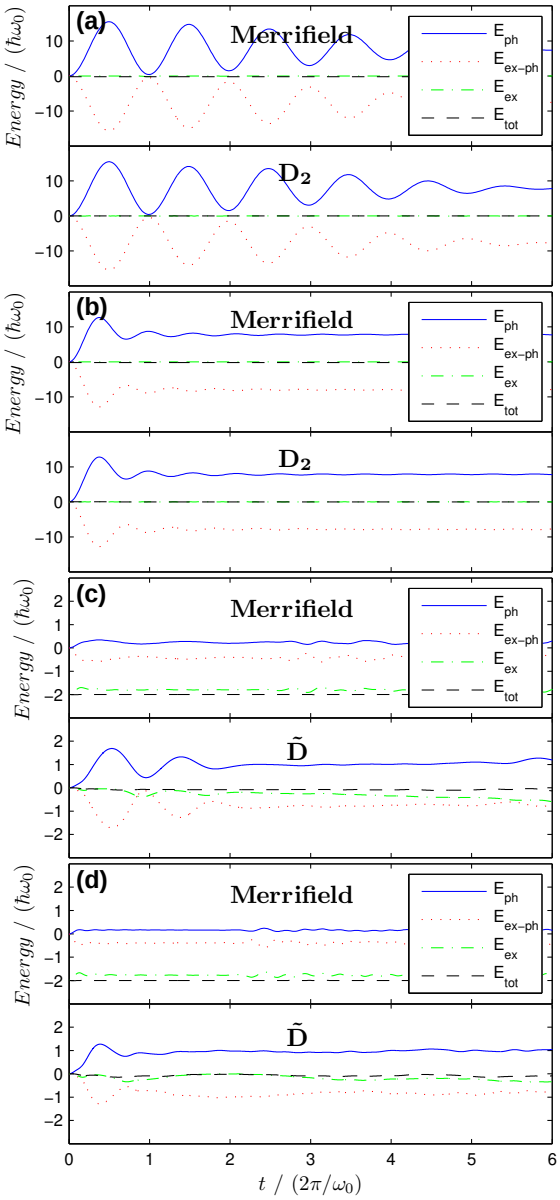


FIG. 11: System energies calculated from the $D_2$ and $\tilde{D}$ Ansätz. The results are compared with those of the Merrifield Ansatz. (a) $J = 0.1$, $W = 0.1$, $S = 4.0$; (b) $J = 0.1$, $W = 0.8$, $S = 4.0$; (c) $J = 1.0$, $W = 0.1$, $S = 0.5$; (d) $J = 1.0$, $W = 0.8$, $S = 0.5$.

small peaks $\omega_{\rm sp}(n_q)$ ($n_q = 0, 1, ..., N/2$):

$$\omega_{\rm sp}(n_q) = \omega_{\rm ZPL} + \omega_0 - W + \frac{4W}{N}n_q \qquad (31)$$

where $\omega_{\rm ZPL}$ is the location of the zero-phonon line. For $W = 0.8\omega_0$ and $N = 32$, $\omega_{\rm sp}(n_q) = \omega_{\rm ZPL} + (0.2 + 0.1 * n_q)\omega_0$ as shown in the inset of Fig. 10b.

Lastly, four cases of system energies calculated from the $D_2$ and $\tilde{D}$ Ansätze are shown in Fig. 11 and compared with those from the Merrifield Ansatz . Since the

Hamiltonian defined in Eq. (1) is time-independent, the total energy of the system is expected to be a constant during the time evolution. At $t = 0$, an exciton is assumed localized at one site and there are no phonons on the entire ring. As shown in Fig. 11, the phonon energy $E_{\rm ph}$ rises from zero and oscillates as time goes on. In the meantime, the interaction energy between the exciton and phonons, $E_{\rm ex-ph}$, oscillates with almost the same amplitude but an opposite sign. And the total energy $E_{\rm tot}$ of the system stays as a constant at all times. As shown in Figs. 11a and 11b, the $D_2$ Ansatz and Merrifield Ansatz agree with each other when $J$ is small and $S$ is large. However, when $J$ is large (e.g., $J = 1.0$) and $S$ is small (e.g., $S = 0.5$), these two Ansätze no longer agree. For this case, the Merrifield Ansatz, which is translationally invariant (a Bloch wave function) but with a built-in small-polaron correlation, is not suitable to describe the dynamics. As shown in Figs. 11c and 11d, the total system energy $E_{\rm tot}$ vanishes during the time evolution of the $\tilde{\rm D}$ Ansatz. While in the Merrifield Ansatz, $E_{\rm tot}$ remains at a constant value $-2$ that is equal to the initial value of $E_{\rm ex}$. This is because in the Merrifield Ansatz, the exciton amplitude is assumed to distribute uniformly over all the sites of the system, thus according to Eq. (2), $E_{\rm ex}$ has a negative value when $J$ is not negligible. However, for an initial state in which the exciton is localized at one site, according to Eq. (2), $E_{\rm ex}$ should be zero at $t = 0$ as shown in Figs. 11c and 11d for the $\tilde{\rm D}$ Ansatz. This shows that the $\tilde{\rm D}$ Ansatz is a more flexible trial state than the Merrifield Ansatz.

Lastly, we give a brief discussion on the validity of the Davydov Ansätze. A Davydov Ansatz is an approximative solution to the Schrödinger equation with the Holstein Hamiltonian. For a trial wave function $|D(t)\rangle$ that does not strictly obey the Schrödinger equation, the deviation vector $|\delta(t)\rangle$ can be written as

$$|\delta(t)\rangle \equiv i\hbar\frac{\partial}{\partial t}|D(t)\rangle - \hat{H}|D(t)\rangle \tag{32}$$

Here $\hat{H}$ is the Holstein Hamiltonian Eq. (1). For the Davydov $D_1$ Ansatz, the explicit form of $|\delta(t)\rangle$[17] was given by Škrinjar *et al.* in 1988. It was also proven that $|\delta(t)\rangle$ is orthogonal to $|D_1(t)\rangle$. However, such orthogonality relations are insufficient to conclude that the deviation vector $|\delta(t)\rangle$ is negligible, and the trial state is a good approximation to the true solution of Schrödinger equation. To have a quantitative measure of the Schrödinger-equation deviation, one needs to calculate the amplitude of the deviation vector $|\delta(t)\rangle$, which is defined as $\Delta(t)$:

$$\Delta(t) \equiv \sqrt{\langle\delta(t)|\delta(t)\rangle} \tag{33}$$

An explicit expression for $\Delta(t)$ as the $D_2$ Ansatz is substituted into the Schrödinger equation is derived in Appendix F.

Note that the dimension of $\Delta(t)$ is that of the energy. Therefore, one can gauge whether the trial state is a good approximative solution by comparing $\Delta(t)$ with the system energies. Two examples of such comparisons for the $D_2$ Ansatz are shown in Figs. 12a and 12b. The control parameters in Figs. 12a and 12b are the same as those in Figs. 11a and 11b, respectively. For both two cases, the main system energies are $E_{\rm ph}$ and $E_{\rm ex-ph}$, and $\Delta(t)$ is found to be negligible to either $E_{\rm ph}$ or $E_{\rm ex-ph}$. We conclude that the $D_2$ Ansatz yields quantitatively accurate solutions to the Schrödinger equation for these two cases.

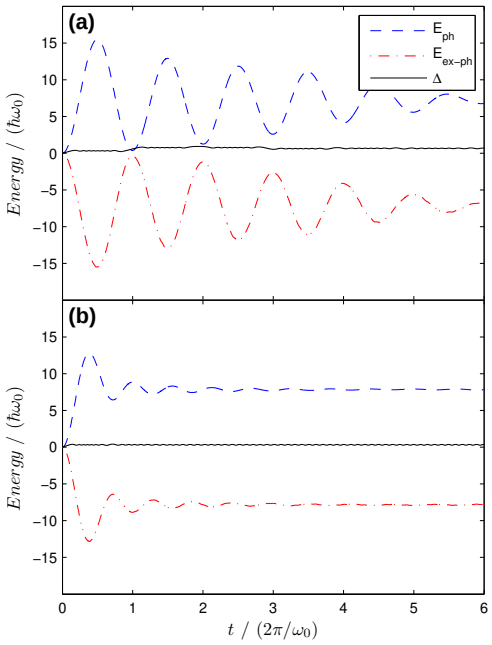


FIG. 12: Amplitude of the deviation vector $|\delta(t)\rangle$ calculated from the $D_2$ Ansatz. The results are compared with the system energies. (a) $J = 0.1$, $W = 0.1$, $S = 4.0$; (b) $J = 0.1$, $W = 0.8$, $S = 4.0$.

## IV. CONCLUSION

In this paper we simulate polaronic dynamics in a one-dimensional molecular chain following the Dirac-Frenkel time-dependent variational approach. After the optical excitation, the coupled exciton-phonon system will undergo a relaxation process from the initial photo-induced nonequilibrium. Based on the Holstein Hamiltonian, we examined time evolution of the exciton amplitude, the reduced exciton density matrix, the exciton coherence size, linear optical absorption, and induced phonon displacements for two types of variational wave functions, namely, the Davydov $D_2$ Ansatz, and a simplified variant of Davydov $D_1$ Ansatz, also known as the $\tilde{\rm D}$ Ansatz. It is shown that following the equations of motion derived from the time-dependent variation, the exciton amplitude will transfer from the site of creation to neighboring sites, and as $J$ increases, the velocity of exciton propagation will increase as well. Exciton-induced phonon deformations can be found to form at the locations where the

exciton has considerable densities, and then propagate to the entire aggregate if there is sufficient phonon dispersion enabling mobility. The half-width of the phonon dispersion, $W$, determines the speeds of phonon wave packets because of a linear phonon dispersion relation given in the model. For a large value of the transfer integral, the left-moving and right-moving wave packets of the exciton departing from the site of creation may make a quick rendezvous at the opposite end of the ring, and therefore, trigger a second pair of localized phonon wave packets. Linear absorption spectra can be derived from the exciton amplitude and the phonon displacements computed from the $D_2$ and $\tilde{D}$ Ansätze. Various system energies are also calculated and analyzed for the one-dimensional coupled exciton-phonon molecular ring after photo-excitation. Overall it is found that $\tilde{D}$ is a more flexible trial state, while the $D_2$ Ansatz is rather efficient for computation, and its extension to higher spatial dimensions is a feasible generalization of our approach.

Our trial states in this paper are both localized wave functions, and we intend to work out detailed dynamics of their translationally invariant counterparts, the Toyozawa Ansatz and the GL Ansatz. Our approaches here can be also readily extended to include other forms of exciton-phonon interactions, such as asymmetric and symmetric off-diagonal coupling[35], and higher-order couplings. Work in this direction is now in progress.


### Acknowledgments

Support from the Singapore Ministry of Education through the Academic Research Fund (Tier 2) under Project No. T207B1214 is gratefully acknowledged.


## APPENDIX A: THE $D_2$ TRIAL STATE

The time evolution equations for $D_1$, $\tilde{D}$ and $D_2$ Ansätze can be derived by employing Dirac-Frenkel time-dependent variation method. We start from the simplest of the three, the $D_2$ Ansatz. For $D_2$ Ansatz, the Lagrangian is defined as

$$\begin{aligned} L &= \langle D_2(t)|\frac{i\hbar}{2}\frac{\overleftrightarrow{\partial}}{\partial t} - \hat{H}|D_2(t)\rangle \\ &= \frac{i\hbar}{2}[\langle D_2(t)|\frac{\overrightarrow{\partial}}{\partial t}|D_2(t)\rangle - \langle D_2(t)|\frac{\overleftarrow{\partial}}{\partial t}|D_2(t)\rangle] \\ &\quad -\langle D_2(t)|\hat{H}|D_2(t)\rangle \end{aligned} \tag{A1}$$

where the first two terms connected with the time derivatives can be calculated as follows

$$\begin{aligned} \langle D_2(t)|\frac{\overrightarrow{\partial}}{\partial t}|D_2(t)\rangle &= \sum_n \psi_n^*\dot{\psi}_n - \sum_n |\psi_n|^2 \sum_q \lambda_q^*\dot{\lambda}_q \\ &\quad + \sum_n |\psi_n|^2 \sum_q [-\frac{1}{2}(\dot{\lambda}_q\lambda_q^* + \lambda_q\dot{\lambda}_q^*)], \end{aligned} \tag{A2}$$

and

$$\begin{aligned} \langle D_2(t)|\frac{\overleftarrow{\partial}}{\partial t}|D_2(t)\rangle &= \sum_n \dot{\psi}_n^*\psi_n - \sum_n |\psi_n|^2 \sum_q \dot{\lambda}_q^*\lambda_q \\ &\quad + \sum_n |\psi_n|^2 \sum_q [-\frac{1}{2}(\dot{\lambda}_q\lambda_q^* + \lambda_q\dot{\lambda}_q^*)] \end{aligned} \tag{A3}$$

The remaining term is the average energy in the $D_2$ trial state:

$$\begin{aligned} \langle D_2|\hat{H}|D_2\rangle &= \langle D_2|\hat{H}_{\rm ex}|D_2\rangle + \langle D_2|\hat{H}_{\rm ph}|D_2\rangle \\ &\quad + \langle D_2|\hat{H}_{\rm ex-ph}|D_2\rangle \end{aligned} \tag{A4}$$

with

$$\langle D_2|\hat{H}_{\rm ex}|D_2\rangle = -J\sum_n \psi_n^*\psi_{n+1} - J\sum_n \psi_n^*\psi_{n-1}$$

$$\langle D_2|\hat{H}_{\rm ph}|D_2\rangle = \sum_n |\psi_n|^2 \sum_q \omega_q|\lambda_q|^2$$

$$\langle D_2|\hat{H}_{\rm ex-ph}|D_2\rangle = \sum_n |\psi_n|^2 \sum_q g_q\omega_q(\lambda_q e^{iqn} + \lambda_q^* e^{-iqn})$$

Equations of motion from the trial wave function $D_2(t)$ are readily obtained from Eq. (23)

$$\begin{aligned} -i\dot{\psi}_n(t) &= \frac{i}{2}\psi_n(t)\sum_q[\dot{\lambda}_q(t)\lambda_q^*(t) - \dot{\lambda}_q^*(t)\lambda_q(t)] \\ &\quad + J\psi_{n+1}(t) + J\psi_{n-1}(t) \\ &\quad - \psi_n(t)\sum_q \omega_q|\lambda_q(t)|^2 \\ &\quad - \psi_n(t)\sum_q g_q\omega_q[\lambda_q(t)e^{iqn} + \lambda_q^*(t)e^{-iqn}] \end{aligned} \tag{A5}$$

$$-i\dot{\lambda}_q(t) = -\sum_n |\psi_n|^2 e^{-iqn} g_q\omega_q - \omega_q\lambda_q \tag{A6}$$

It can easily be shown the norm of the $D_2$ trial state is conserved, i.e.,

$$\frac{d}{dt}[\sum_{n=1}^{N} |\psi_n(t)|^2] = 0 \tag{A7}$$

And in this paper, we set

$$\sum_{n=1}^{N}|\psi_n(t)|^2=1 \tag{A8}$$

Solutions to Eq. (A5) and (A6) provide the dynamic information of the exciton-phonon system.

## APPENDIX B: THE $\tilde{\mathrm{D}}$ TRIAL STATE

For the $\tilde{\mathrm{D}}$ trial state, the localized backbone of the translationally-invariant GL Ansatz, we can also derive coupled equation for the time-dependent variational parameters using the Lagrangian formalism

$$\begin{aligned}L &= \langle\tilde{D}(t)|\frac{i\hbar}{2}\frac{\overleftrightarrow{\partial}}{\partial t}-\hat{H}|\tilde{D}(t)\rangle\\ &= \frac{i\hbar}{2}[\langle\tilde{D}(t)|\frac{\overrightarrow{\partial}}{\partial t}|\tilde{D}(t)\rangle-\langle\tilde{D}(t)|\frac{\overleftarrow{\partial}}{\partial t}|\tilde{D}(t)\rangle]\\ &\quad -\langle\tilde{D}(t)|\hat{H}|\tilde{D}(t)\rangle\end{aligned} \tag{B1}$$

wherein the individual terms can be calculated as follows

$$\begin{aligned}&\langle\tilde{D}(t)|\frac{\overrightarrow{\partial}}{\partial t}|\tilde{D}(t)\rangle\\ &= \sum_n\psi_n^*\dot{\psi}_n+\sum_n|\psi_n|^2[N^{-1}\sum_q(\dot{\beta}_qe^{-iqn}\\ &\quad -\dot{\lambda}_q)(\beta_q^*e^{iqn}-\lambda_q^*)]+\sum_n|\psi_n|^2\\ &\quad [-\frac{1}{2}N^{-1}\sum_q(\dot{\beta}_qe^{-iqn}-\dot{\lambda}_q)(\beta_q^*e^{iqn}-\lambda_q^*)\\ &\quad +(\beta_qe^{-iqn}-\lambda)(\dot{\beta}_q^*e^{iqn}-\dot{\lambda}_q)]\end{aligned} \tag{B2}$$

$$\begin{aligned}&\langle\tilde{D}(t)|\frac{\overleftarrow{\partial}}{\partial t}|\tilde{D}(t)\rangle\\ &= \sum_n\dot{\psi}_n^*\psi_n+\sum_n|\psi_n|^2[N^{-1}\sum_q(\dot{\beta}_q^*e^{iqn}\\ &\quad -\dot{\lambda}_q^*)(\beta_qe^{-iqn}-\lambda_q)]+\sum_n|\psi_n|^2\\ &\quad [-\frac{1}{2}N^{-1}\sum_q(\dot{\beta}_qe^{-iqn}-\dot{\lambda}_q)(\beta_q^*e^{iqn}-\lambda_q^*)\\ &\quad +(\beta_qe^{-iqn}-\lambda)(\dot{\beta}_q^*e^{iqn}-\dot{\lambda}_q)]\end{aligned} \tag{B3}$$

and

$$\langle\tilde{D}|\hat{H}|\tilde{D}\rangle = \langle\tilde{D}|\hat{H}_{\mathrm{ex}}|\tilde{D}\rangle+\langle\tilde{D}|\hat{H}_{\mathrm{ph}}|\tilde{D}\rangle+\langle\tilde{D}|\hat{H}_{\mathrm{ex-ph}}|\tilde{D}\rangle \tag{B4}$$

with

$$\langle\tilde{D}|\hat{H}_{\mathrm{ex}}|\tilde{D}\rangle=-J\sum_n\psi_n^*(\psi_{n+1}S_{n,n+1}+\psi_{n-1}S_{n,n-1})$$

$$\langle\tilde{D}|\hat{H}_{\mathrm{ph}}|\tilde{D}\rangle=N^{-1}\sum_n|\psi_n|^2\sum_q\omega_q|\beta_qe^{-iqn}-\lambda_q|^2$$

$$\begin{aligned}\langle\tilde{D}|\hat{H}_{\mathrm{ex-ph}}|\tilde{D}\rangle &= N^{-1/2}\sum_n|\psi_n|^2\sum_qg_q\omega_q[(\beta_q^*e^{iqn}-\lambda_q^*)\\ &\quad e^{-iqn}+(\beta_qe^{-iqn}-\lambda_q^*)e^{-iqn}].\end{aligned}$$

Substituting Eqs. (B1)-(B4) into Eq. (23), one arrives at the equations of time evolution for the $\tilde{\mathrm{D}}$ Ansatz:

$$\begin{aligned}-i\dot{\psi}_n(t) &= \frac{i}{2}N^{-1}\psi_n\sum_q[(\dot{\beta}_qe^{-iqn}-\dot{\lambda_q})(\beta_q^*e^{iqn}-\lambda_q^*)\\ &\quad -(\dot{\beta}_q^*e^{iqn}-\dot{\lambda}_q^*)(\beta_qe^{-iqn}-\lambda_q)]\\ &\quad +J\psi_{n+1}S_{n,n+1}+J\psi_{n-1}S_{n,n-1}\\ &\quad -N^{-1}\psi_n\sum_q\omega_q|\beta_qe^{-iqn}-\lambda_q|^2-N^{-1/2}\psi_n\\ &\quad \sum_qg_q\omega_q[\beta_q^*-\lambda_q^*e^{iqn}+\beta_q-\lambda_qe^{iqn}]\end{aligned} \tag{B5}$$

$$\begin{aligned}-iN^{-1}&\sum_n|\psi_n|^2\dot{\lambda}_q(t)=\\ &-i\sum_n|\psi_n|^2\dot{\beta}_qe^{-iqn}N^{-1}\\ &+\frac{1}{2}N^{-1}J\sum_n\psi_n^*\psi_{n+1}S_{n,n+1}\\ &\beta_q[e^{-iqn}-e^{-iq(n+1)}]\\ &+\frac{1}{2}N^{-1}J\sum_n\psi_n^*\psi_{n-1}S_{n,n-1}\\ &\beta_q[e^{-iqn}-e^{-iq(n-1)}]\\ &+N^{-1}\sum_n|\psi_n|^2\omega_q(\beta_qe^{-iqn}-\lambda_q)\\ &+N^{-1/2}\sum_n|\psi_n|^2g_q\omega_qe^{-iqn}\end{aligned} \tag{B6}$$

$$\begin{aligned}-iN^{-1}&\sum_n|\psi_n|^2\dot{\beta}_q=\\ &-iN^{-1}\sum_n|\psi_n|^2\dot{\lambda}_qe^{iqn}\\ &+JN^{-1}\sum_n\psi_n^*\psi_{n+1}S_{n,n+1}\\ &[\beta_q(e^{-iq}-1)+\frac{1}{2}\lambda_qe^{iqn}(e^{iq}-1)]\\ &+JN^{-1}\sum_n\psi_n^*\psi_{n-1}S_{n,n-1}\\ &[\beta_q(e^{iq}-1)+\frac{1}{2}\lambda_qe^{iqn}(e^{-iq}-1)]\\ &-N^{-1}\sum_n|\psi_n|^2\omega_q(\beta_q-\lambda_qe^{iqn})\\ &-N^{-1/2}\sum_n|\psi_n|^2g_q\omega_q\end{aligned} \tag{B7}$$

## APPENDIX C: THE $D_1$ TRIAL STATE

The same procedure in Appendices A and B can be applied to the $D_1$ Ansatz[36] with variational parameters $\psi_n$ and $\lambda_{qn}$, and one can obtain

$$\begin{aligned} -i\dot{\psi}_n(t) &= \frac{i}{2}N^{-1}\psi_n\sum_q[\dot{\lambda}_{qn}\lambda^*_{qn}-c.c.] \\ &+J\psi_{n+1}S_{n,n+1}+J\psi_{n-1}S_{n,n-1} \\ &-N^{-1/2}\psi_n\sum_q g_q\omega_q[\lambda_{qn}e^{iqn}+c.c.] \\ &-N^{-1}\psi_n\sum_q\omega_q|\lambda_{qn}|^2 \end{aligned} \tag{C1}$$

$$\begin{aligned} -iN^{-1}\quad & |\psi_n|^2\dot{\lambda}_{qn}(t)= \\ & +N^{-1}J\psi^*_n\psi_{n+1}(\lambda_{q,n+1}-\lambda_{qn})S_{n,n+1} \\ & +N^{-1}J\psi^*_n\psi_{n-1}(\lambda_{q,n-1}-\lambda_{qn})S_{n,n-1} \\ & -N^{-1}|\psi_n|^2\omega_q\lambda_{qn} \\ & -N^{-1/2}|\psi_n|^2 g_q\omega_q e^{-iqn} \end{aligned} \tag{C2}$$

These coupled differential equations can be numerically solved by the fourth-order Runge-Kutta method, and work on this is now in progress.

## APPENDIX D: NUMERICAL DETAILS

There are various numerical approaches to solve coupled differential equations such as Eqs. (A5) and (A6) for the $D_2$ Ansatz and Eqs. (B5), (B6) and (B7) for the $\tilde{D}$ Ansatz. One way is to transform these equations into the Volterra integral equations[37] for minimization purposes, and then use a nonlinear optimization method such as the Newton-Raphson method to solve them. Another approach is to solve the time-dependent differential equations directly. The latter method has a much higher computational efficiency, but it requires a higher precision in the single iterative time step since the computational error may accumulate as the number of the iterative steps increases.

In this paper, we use the Runge-Kutta fourth-order method[38,39] to solve Eqs. (A5) and (A6) and Eqs. (B5), (B6) and (B7). The Runge-Kutta fourth-order method is widely used to solve differential equations. Its single step error is fifth order, i.e., $O(\Delta t^5)$. The algorithm for this method can be described as follows:

$$\begin{aligned} k_1 &= f(t_n,\alpha(t_n))\Delta t \\ k_2 &= f(t_n+\frac{1}{2}\Delta t,\alpha(t_n)+\frac{1}{2}k_1)\Delta t \\ k_3 &= f(t_n+\frac{1}{2}\Delta t,\alpha(t_n)+\frac{1}{2}k_2)\Delta t \\ k_4 &= f(t_n+\Delta t,\alpha(t_n)+k_3)\Delta t \\ \alpha(t_{n+1}) &= \alpha(t_n)+\frac{k_1}{6}+\frac{k_2}{3}+\frac{k_3}{3}+\frac{k_4}{6}+O(\Delta t^5) \end{aligned}$$

where

$$f(t_n,\alpha(t_n))=\frac{d\alpha(t_n)}{dt_n}$$

and from $t_n$ to $t_{n+1}\equiv t_n+\Delta t$.

For the $D_2$ Ansatz, $\alpha$ represents $\psi_n$ or $\lambda_q$, and is obtained by Eqs. (A5) and (A6). Then, by calculating $k_1$, $k_2$, $k_3$ and $k_4$, one can get the parameters $\alpha(t_{n+1})$ for the next time step using the fourth-order Runge-Kutta method.

## APPENDIX E: LINEAR ABSORPTION SPECTRUM BY $D_2$ AND $\tilde{D}$ ANSÄTZE

The linear absorption spectrum of the exciton-phonon system studied in this paper is calculated by

$$\widetilde{F}(\omega)=\frac{1}{\pi}\mathrm{Re}\int_0^\infty F(t)e^{i\omega t}dt \tag{E1}$$

with

$$F(t)= {}_{\rm ph}\langle 0|_{\rm ex}\langle 0|\hat{P}e^{-i\hat{H}t}\hat{P}^\dagger|0\rangle_{\rm ex}|0\rangle_{\rm ph} \tag{E2}$$

where $\hat{P}$ is the polarization operator

$$\hat{P}=\mu\sum_n(|n\rangle_{\rm ex}\ {}_{\rm ex}\langle 0|+|0\rangle_{\rm ex}\ {}_{\rm ex}\langle n|) \tag{E3}$$

Here $\mu$ is the transition dipole matrix element for a single site, and $|n\rangle_{\rm ex}$ is the exciton state at the $n$th site $|n\rangle_{\rm ex}\equiv\hat{a}^\dagger_n|0\rangle_{\rm ex}$.

Substituting Eq. (E3) into Eq. (E2) one obtains

$$F(t)=\mu^2\sum_n\sum_m\ {}_{\rm ph}\langle 0|_{\rm ex}\langle m|e^{-i\hat{H}t}|n\rangle_{\rm ex}|0\rangle_{\rm ph} \tag{E4}$$

wherein $e^{-i\hat{H}t}|n\rangle_{\rm ex}|0\rangle_{\rm ph}$ can be approximated by a Davydov trial state, for example, by a $D_2$ trial state:

$$\begin{aligned} & e^{-i\hat{H}t}|n\rangle_{\rm ex}|0\rangle_{\rm ph}\approx \\ & \sum_{n'}\psi_{n'-n}(t)|n'\rangle_{\rm ex} \\ & \times\exp(\sum_q[\lambda_q(t)\hat{b}^\dagger_q-\lambda^*_q(t)\hat{b}_q])|0\rangle_{\rm ph} \end{aligned} \tag{E5}$$

where the variational parameters $\psi_{n'-n}(t)$ ($n'=0,2,...,N-1$) and $\lambda_q(t)(q=-N/2+1,-N/2+2,...,N/2)$ have the following initial values

$$\psi_{n'-n}(t=0)=\delta_{n'-n}, \tag{E6}$$

and

$$\lambda_q(t=0)=0. \tag{E7}$$

Substituting Eq. (E5) into Eq. (E4), we obtain the formula to calculate $F(t)$ by $D_2$ Ansatz:

$$\begin{aligned} F(t) &= \mu^2 \sum_n \sum_m \psi_m(t) \\ &\quad \times {}_{\rm ph}\langle 0| \exp(\sum_q [\lambda_q(t)\hat{b}_q^\dagger - \lambda_q^*(t)\hat{b}_q])|0\rangle_{\rm ph} \\ &= \mu^2 \sum_n \sum_m \psi_m(t) \exp(-\frac{1}{2}\sum_q |\lambda_q(t)|^2) \\ &= \mu^2 N \sum_m \psi_m(t) \exp(-\frac{1}{2}\sum_q |\lambda_q(t)|^2) \end{aligned} \tag{E8}$$

wherein $\lambda_q(t)$ and $\psi_m(t)$ are initialized by Eq. (E7) and Eq. (E6) (i.e., $\psi_m(0) = \delta_{m,0}$) and then solved by Eqs. (A6) and (A5).

The same procedure from Eq.(E5) to (E8) can be applied to $\tilde{\rm D}$ Ansatz, and one obtains

$$F(t) = \mu^2 N \sum_m \psi_m(t) \exp(-\frac{1}{2}\sum_q |\beta_q(t)e^{-iqm} - \lambda_q(t)|^2) \tag{E9}$$

where the variational parameters $\psi_m(t)$, $\beta_q(t)$ and $\lambda_q(t)$ are solved by Eqs. (B5)-(B7) with the initial values $\psi_m(0) = \delta_{m,0}$, $\beta_q(0) = 0$ and $\lambda_q(0) = 0$.

## APPENDIX F: DEVIATION VECTOR OF THE $D_2$ ANSATZ

Substituting Eqs. (1)-(4), (15) and (16) into Eq. (32), one obtains the expression of $|\delta(t)\rangle$ for the $D_2$ Ansatz:

$$\begin{aligned} |\delta(t)\rangle &= \sum_n \hat{B}_n^\dagger \{ i\{ \dot{\psi}_n(t) + \\ &\quad \psi_n(t) \sum_q \{\hat{b}_q^\dagger \dot{\lambda}_q(t) - {\rm Re}[\dot{\lambda}_q(t)\lambda_q^*(t)]\}\} \\ &\quad + J[\psi_{n+1}(t) + \psi_{n-1}(t)] - \psi_n(t)\sum_q \omega_q \hat{b}_q^\dagger \lambda_q(t) \\ &\quad + \psi_n(t) \sum_q g_q\omega_q [\hat{b}_q^\dagger e^{-inq} + \lambda_q(t)e^{inq}]\} \\ &\quad \exp(\sum_q [\lambda_q(t)\hat{b}_q^\dagger - \lambda_q^*(t)\hat{b}_q])|0\rangle_{\rm ph}|0\rangle_{\rm ex} \end{aligned} \tag{F1}$$

Then, the expression of $\langle\delta(t)|\delta(t)\rangle$ for the $D_2$ Ansatz can be obtained:

$$\begin{aligned} &\langle\delta(t)|\delta(t)\rangle = J^2 \sum_n |\psi_{n+1}(t) + \psi_{n-1}(t)|^2 \\ &-2J[\sum_q \omega_q |\lambda_q(t)|^2]{\rm Re}[\sum_n [\psi_{n+1}^*(t) + \psi_{n-1}^*(t)]\psi_n(t)] \\ &+4J{\rm Re}[\sum_n [\psi_{n+1}^*(t) + \psi_{n-1}^*(t)]\theta_n(t)] \\ &-2J{\rm Re}[\sum_n [\psi_{n+1}^*(t) + \psi_{n-1}^*(t)]\vartheta_n(t)] \\ &+[\sum_n |\psi_n(t)|^2]\{[\sum_q \omega_q|\lambda_q(t)|^2]^2 + \sum_q |\omega_q\lambda_q(t)|^2\} \\ &-4[\sum_q \omega_q|\lambda_q(t)|^2]^2 \sum_n \psi_n^*(t)\theta_n(t) \\ &-2\sum_n \psi_n^*(t)\psi_n(t)\sum_q g_q\omega_q^2 {\rm Re}[\lambda_q(t)e^{inq}] \\ &+2[\sum_q \omega_q|\lambda_q(t)|^2]{\rm Re}[\sum_n \psi_n^*(t)\vartheta_n(t)] \\ &+2[\sum_n |\psi_n(t)|^2]{\rm Im}[\sum_q \omega_q \dot{\lambda}_q(t)\lambda_q^*(t)] \\ &+4\sum_n |\theta_n(t)|^2 + [\sum_n |\psi_n(t)|^2]\sum_q (g_q\omega_q)^2 \\ &-4{\rm Re}[\sum_n \theta_n^*(t)\vartheta_n(t)] \\ &-2{\rm Im}[\sum_n \psi_n^*(t)\psi_n(t)\sum_q g_q\omega_q\dot{\lambda}_q(t)e^{inq}] \\ &+\sum_n |\vartheta_n(t)|^2 + [\sum_n |\psi_n(t)|^2]\sum_q |\dot{\lambda}_q(t)|^2 \end{aligned} \tag{F2}$$

where

$$\theta_n(t) \equiv \psi_n(t)\sum_q g_q\omega_q {\rm Re}[\lambda_q(t)e^{inq}] \tag{F3}$$

and

$$\vartheta_n(t) \equiv \psi_n(t){\rm Im}[\sum_q \dot{\lambda}_q(t)\lambda_q^*(t)] - i\dot{\psi}_n(t) \tag{F4}$$


[1] Z. An, C. Q. Wu, X. Sun, Phys. Rev. Lett **93**, 216407 (2004).
[2] B. Zheng, J. Wu, W. Sun, C. Liu, Chem. Phys. Lett **425**, 123 (2006).
[3] X. Liu, K. Gao, J. Fu, Y. Li, J. Wei, and S. Xie, Phys. Rev. B **74**, 172301 (2006).
[4] S. Tomimoto, H. Nansei, S. Saito, T. Suemoto, J. Takeda, S. Kurita, Phys. Rev. Lett. **81**, 417 (2000).
[5] R.E. Merrifield, J. Chem. Phys. **40**, 4450 (1964).
[6] Y. Zhao, D.W. Brown, and K. Lindenberg, J. Chem. Phys. **106**, 5622 (1997).
[7] S. Tanaka, Y, Kayanuma, J. Lumin. **87**, 936 (2000).
[8] S. Tanaka, J. Chem. Phys **119**, 4891 (2003).
[9] Y. Zhao, D. W. Brown, and K. Lindenberg, J. Chem. Phys. **106**, 2728 (1997).
[10] Yutaka Toyozawa, Prog. Theor. Phys. **26**, 29-44 (1961).
[11] Y. Zhao, Doctoral Thesis, University of California, San Diego, 1994.
[12] Y. Zhao, D. W. Brown, and K. Lindenberg, J. Chem. Phys. **107**, 3159 (1997); **107**, 3179 (1997).

[13] Y. Zhao *et al.*, in preparation.
[14] Y. Zhao, G. Li, J. Sun, W.H. Wang, J. Chem. Phys. **129**, 124114 (2008).
[15] A.S. Davydov and N.I. Kislukha, Zh. Eksp. Teor. Fiz. **71**, 1090 (1976) [Sov. Phys. JETP **44**, 571 (1976)].
[16] A.S. Davydov, *Solitons in Molecular Systems* (Reidel, Dordrecht, 1985).
[17] M. J. Škrinjar, D. V. Kapor, and S. D. Stojanović, Phys. Rev. A **38** 6402 (1988).
[18] W. Förner, J. Phys.: Condens. Matter **5** 3897 (1993).
[19] L. Cruzeizo-Hansson, Phys. Rev. Lett. **73** 2927 (1994).
[20] L. Cruzeizo-Hansson and S. Takeno, Phys. Rev. E **56** 894 (1997).
[21] A.M. Clogston, Phys. Rev. E **58** 6407 (1998).
[22] S. Gheorghiu-Svirschevski, Phys. Rev. E **64** 051907 (2001).
[23] L. Cruzeiro, J. Biol. Phys. **35** 43 (2009).
[24] P.A.M. Dirac, Proc. Cambridge, Phil. Soc. **26**, 376 (1930); J. Frenkel, *Wave Mechanics* (Oxford Univ. Press, 1934).
[25] H. Frölich, Proc. R. Soc. London, Ser. A **215**, 291 (1952); Adv. Phys. **3**, 325 (1954).
[26] T. Holstein, Ann. Phys. (N.Y.) **8**, 325 (1959); **8**, 343 (1959).
[27] G. D. Manhan *Many-Particle Physics* (Plenum, New York, 1990).
[28] N. Lu and S. Mukamel, J. Chem. Phys. **95**, 1588 (1991).
[29] S. Mukamel, *Principles of Nonlinear Optical Spectroscopy* (Oxford, New York, 1995)
[30] K. Huang and A. Rhys, Proc. R. Soc. London, Ser. A **204**, 406 (1950).
[31] C. Itzykson and J. Zuber, *Many-Particle Physics*, McGraw-Hill Inc (1980).
[32] T. Meier, Y. Zhao, V. Chernyak, and S. Mukamel, J. Chem. Phys. **107** 3876 (1997).
[33] Y. Zhao, T. Meier, W. M. Zhang, V. Chernyak, and S. Mukamel, J. Phys. Chem. B **103**, 3954 (1999).
[34] Y. Zhao *et al.*, J. Chem. Phys. **113**, 6502 (2000).
[35] Y. Zhao, D.W. Brown, and K. Lindenberg, J. Chem. Phys. **100**, 2335 (1994).
[36] Y. Zhao, S. Yokojima, and G. Chen, J. Chem. Phys. **113**, 4016 (2000).
[37] G. Grippenberg, S.O. Londen and O. Staffans, *Volterra integral and functional equations*, Cambridge University Press (1990).
[38] C.W. Gear, *Numerical Initial Value Problems in Ordinary Differential Equations* (Englewood Cliffs, NJ: Prentice-Hall, 1971), Chapter 2.
[39] J. D. Lambert, *Numerical methods for ordinary differential systems: the initial value problem*, John Wiley & Sons, Inc., New York, NY (1991).